International Journal of Nanomedicine

Dovepress
open access to scientific and medical research

Open Access Full Text Article

ORIGINAL RESEARCH

Effects of green synthesised silver nanoparticles (ST06-AgNPs) using curcumin derivative (ST06) on human cervical cancer cells (HeLa) in vitro and EAC tumor bearing mice models

This article was published in the following Dove Press journal:
International Journal of Nanomedicine

Kalaimathi Murugesan[1,*]
Jinsha Koroth[1,2,*]
Padma Priya Srinivasan[1]
Amrita Singh[3]
Sanjana Mukundan[1]
Subhas S Karki[4]
Bibha Choudhary[1]
Chhitar M Gupta[1]

[1]Institute of Bioinformatics and Applied Biotechnology (IBAB), Bangalore, India; [2]Department of Pharmaceutical Chemistry, Manipal Academy of Higher Education, Manipal 576104, Karnataka, India; [3]Water Analysis Laboratory, Nanomaterial Toxicology Group, CSIR-Indian Institute of Toxicology Research, Lucknow, India; [4]KLE Academy of Higher Education & Research, KLE College of Pharmacy, Bangalore, KN, India

*These authors contributed equally to this work

Background: In recent years, green synthesized silver nanoparticles have been increasingly investigated for their anti-cancer potential. In the present study, we aimed at the biosynthesis of silver nanoparticles (AgNPs) using a curcumin derivative, ST06. Although, the individual efficacies of silver nanoparticles or curcumin derivatives have been studied previously, the synergistic cytotoxic effects of curcumin derivative and silver nanoparticles in a single nanoparticulate formulation have not been studied earlier specifically on animal models. This makes this study novel compared to the earlier synthesized curcumin derivative or silver nanoparticles studies. The aim of the study was to synthesize ST06 coated silver nanoparticles (ST06-AgNPs) using ST06 as both reducing and coating agent.

Methods: The synthesized nanoparticles AgNPs and ST06-AgNPs were characterised for the particle size distribution, morphology, optical properties and surface charge by using UV-visible spectroscopy, dynamic light scattering (DLS) and transmission electron microscopy (TEM). Elemental composition and structural properties were studied by energy dispersive X-ray spectroscopy (EDX) and X-ray diffraction spectroscopy (XRD). The presence of ST06 as capping agent was demonstrated by Fourier transform infrared spectroscopy (FTIR).

Results: The synthesized nanoparticles (ST06-AgNPs) were spherical and had a size distribution in the range of 50–100 nm. UV-Vis spectroscopy displayed a specific silver plasmon peak at 410 nm. The in vitro cytotoxicity effects of ST06 and ST06-AgNPs, as assessed by MTT assay, showed significant growth inhibition of human cervical cancer cell line (HeLa). In addition, studies carried out in EAC tumor-induced mouse model (Ehrlich Ascites carcinoma) using ST06-AgNPs, revealed that treatment of the animals with these nanoparticles resulted in a significant reduction in the tumor growth, compared to the control group animals.

Conclusion: In conclusion, green synthesized ST06-AgNPs exhibited superior anti-tumor efficacy than the free ST06 or AgNPs with no acute toxicity under both in vitro and in vivo conditions. The tumor suppression is associated with the intrinsic apoptotic pathway. Together, the results of this study suggest that ST06-AgNPs could be considered as a potential option for the treatment of solid tumors.

Keywords: silver nanoparticles, anticancer, Ehrlich Ascites carcinoma, apoptosis

Correspondence: Kalaimathi Murugesan
Institute of Bioinformatics and Applied Biotechnology (IBAB), Biotech Park, Electronic City Phase I, Bangalore, KN 560100, India
Tel +91 958 598 6415
Email mathi.biotech@gmail.com

Introduction

Curcumin a biphenyl compound, isolated from the rhizomes of turmeric (Curcuma longa) is widely known for its multiple medicinal properties[1], including the anti-cancer property. Despite notable chemo preventive effects of curcumin, its low water solubility and poor

bioavailability markedly limit its clinical uses.[2] Several approaches have been examined to overcome these limitations and to improve the bioactivity of curcumin. One such approach is the synthesis of curcumin derivatives or analogues that have higher bioavailability. Recent studies have shown that some of the curcumin derivatives exhibit significantly stronger anticancer activity than that of curcumin.[3–8] One example of such compounds is 3,4,5-trimethoxy derivatives of curcumin, especially bis[(3E,5E)-4-oxo-3,5-bis[(3,4,5-trimethoxyphenyl) methylene]-1-piperidyl ethane-1,2-dione, which have been reported to exhibit higher metabolic stability and cytotoxic potency, compared to curcumin.[9] In the present study we have synthesized the known compound (1,2-bis[(3E,5E)-4-oxo-3,5-bis[(3,4,5-trimethoxyphenyl) methylene]-1-piperidyl] ethane-1,2-dione), which is referred here as ST06, and its anticancer potential has been analysed after loading it on AgNPs.

Earlier studies have suggested that intervention with curcumin loaded nanoparticulate systems presents several benefits, including improved solubility, enhanced drug uptake, and site-specific delivery.[10] In recent years, plant-mediated biosynthesis of silver nanoparticles (AgNPs) has received considerable attention owing to its simple, non-toxic and eco-friendly way of synthesis. The method of green synthesis of AgNPs, using plant extracts not only make them more sustainable and biocompatible[11–13] but it may also result in functionalization of the nanoparticles, which could further enhance their anti-cancer activity.[14]

Several studies have evaluated the anti-cancer potential of green AgNPs on cancer cell lines and animal models.[15–20] These nanoparticles exhibited anti-cancer effects on a variety of cancer cell lines, such as breast cancer,[21] lung cancer,[22] colon cancer[23] and cervical cancer.[21] Biogenic AgNPs inhibited the cervical carcinoma cells by caspase mediated cell death[24] and nanosilver induced apoptosis via mitochondrial pathway.[25] Another study which elucidated the possible mechanism of cytotoxicity of AgNPs on human fibroblast cells (IMR-90) and glioblastoma cells (U251) showed that these nanoparticles increased the production of reactive oxygen species (ROS), which resulted in DNA damage and cell cycle arrest.[26] These results suggest that AgNPs have great potential in anti-cancer therapeutics. However, more studies are needed to understand the underlying molecular mechanism attributing to their therapeutic efficacy.

Unlike in vitro studies, only limited studies have evaluated the antitumor potential of AgNPs in animal models. AgNPs exhibited potent antiangiogenic ability by inhibiting the vascular endothelial growth factor (VEGF) in retinal endothelial cells.[27] It has been reported that AgNPs exert their anti-angiogenic activity through activation of P13K/Akt signalling pathways.[28] Treatment of lymphosarcoma tumor bearing animals with AgNPs significantly increased their survival period, as compared to the control group.[29] In a similar study, AgNPs have been shown to significantly increase (by about 50%) the survival of Dalton's lymphoma ascites tumor-bearing mice, and decreased (by about 60%) the ascitic fluid in the tumor.[30,31] In the present study, we utilised ST06, a curcumin derivative as reducing agent for the synthesis of silver nanoparticles (AgNPs) and later ST06 was coated on to the synthesised AgNPs. The ST06-AgNPs thus-synthesised were characterised by ultraviolet-visible (UV-Vis) spectroscopy, dynamic light scattering (DLS), transmission electron microscopy (TEM), energy dispersive X-ray spectroscopy (EDX), and Fourier-transform infrared spectroscopy (FTIR). The anticancer activity of ST06-AgNPs was evaluated in human cervical cancer cell line (HeLa) as well as in Ehrlich's ascites carcinoma (EAC) tumor bearing mice.

Materials and methods

Synthesis of ST06

The reaction of 4-piperidone hydrochloride with 3,4,5, -trimethoxy benzaldehydes in the presence of dry hydrogen chloride yielded 3,4,5-bis(benzylidene)-4-piperidone. To a solution of respective 3,5-dibenzyledenepiperidin-4-one (0.024 M) in acetone (25 ml), potassium carbonate (0.04) was added. To this reaction mixture, tetrabutyl ammonium bromide (TBAB) (0.002 M) was added and then the reaction mixture was stirred at room temperature for 1 hr. To this reaction mixture, oxalyl chloride (0.012 M, 2.2 ml) was added dropwise. The reaction mixture was stirred at room temperature for 24 hrs. The product obtained was filtered, washed with water and recrystallized from ethanol (Figures S1 and S2).

Preparation of AgNPs

The biosynthesis of AgNPs followed the protocol mentioned by Yang et al.[32] Briefly, 250 µL of 20 mM ST06 dissolved in DMSO was mixed with 22.5 mL millipore water and the pH was adjusted to alkaline with KOH. With vigorous stirring at 100°C, 2.5 mL $AgNO_3$ (10 mM) was quickly added to the mixture (Figure 3). The colour changed from yellow to brown after a few minutes. The mixture was stirred at

100°C for 1 hr and then cooled down to room temperature. AgNPs thus prepared were collected by centrifugation at 16,000 rpm for 20 mins, and then washed several times with deionized water to remove any unreacted silver and ST06. UV–visible spectroscopy was used to detect the surface plasmon resonance (LSPR) peaks for silver nanoparticles. The synthesised AgNPs were dried.

Preparation of ST06-bound AgNPs

In order to prepare ST06 bound silver nanoparticles (ST06-AgNPs), the protocol mentioned by Ahmed et al.[33] was followed. Briefly, 5 mL of ST06 solution (200 µg/mL) was added to a 50 mL suspension of silver nanoparticles (AgNPs). The reaction mixture was sonicated for 2 mins and magnetically stirred for 24 hrs at room temperature. UV–visible spectroscopy was used to detect the position of silver plasmon peaks for ST06-adsorbed AgNPs. The reaction mixture was centrifuged at 12,000 rpm for 10 mins and the pellet (ST06-AgNPs) obtained was washed twice with distilled water. Finally, the nanoparticles were freeze-dried and were stored at room temperature (26 °C) for further study.

Characterization of ST06-AgNPs

The reaction mixture was scanned in the range of 200 – 8[illegible]nm for AgNPs and ST06-AgNPs respectively, in a UV-Vis spectrophotometer (Tecan infinite M 200 p[illegible], Tec[illegible] Austri[illegible] GmbH, Grödig, Austria). The shape, m[illegible]hology [illegible]d dispersal of the nanoparticles were anal[illegible]sed b[illegible]M. The size distribution profile and the zeta [illegible]ential of the [illegible]anoparticles were analysed using DLS with [illegible]particle size analyser (Malvern zetasizer nano [illegible]S90, Malvern[illegible]K). The elemental composition and crys[illegible]line nature of silver nanoparticles were determined by [illegible]ray diffraction (Powder X-ray—D8 advanced diff[illegible]tomet[illegible] BRUK[illegible]R). FT-IR spectra was recorded [illegible] a sin[illegible]le beam [illegible]olet iS5 FT-IR spectrophotometer [illegible]with t[illegible] following parameters: scan range, 4000–500 [illegible]; number of scans, 16; and resolution 4.0 cm^{-1}.

Transmiss[illegible] Electron Microscope (TEM) samples were prepared by placing a drop of dispersed NPs solution onto formvar coated copper grid for determining morphology and polydispersity in particle size. The micrographs were obtained on TECNAI G2 Spirit (FEI, Netherland) equipped with Gatan digital camera operated at an accelerating voltage at 80 kV. Elemental composition of the NPs was analysed by placing the drop of nanoparticle solution on aluminium stub and elemental analysis was done using Field Emission Scanning Electron Microscope (FE-SEM) coupled with Energy Dispersive X-ray analysis (EDAX) on Quanta FEG 450 (FEI, Netherland).

Cancer cell culture

Human cervical cancer cell lines (HeLa) was purchased from NCCS (National center for cell sciences), Pune, India. Cells were grown in MEM with 10% Fetal bovine serum and antibiotic-antimycotic agents (GIBCO, Thermo fisher scientific, US) at 37°C in a humidified incubator with 5% CO_2 supply.

MTT assay

The in vitro cytotoxicity o[illegible]T06 and S[illegible]06-AgNPs on human cancer cell lin[illegible] were [illegible]sessed [illegible] MTT (3-(4, 5-dimethylthiazol-2-[illegible])-2–5-diphenyl[illegible]tr[illegible]olium bromide) assay. Briefly, He[illegible] cells [illegible]ere plated at a concentration of 5×10^3 in [illegible]6-well[illegible]ate (NE[illegible]®, New Jessey, USA). After 24 [illegible] the cells w[illegible]e [illegible]ubjected to treatment with ST06 and ST06 [illegible]gNPs for 48 hrs (0.5 µM, 1 µM, 1.5 µM, and [illegible]M). After t[illegible] incubation, 10 ul of MTT (5 mg/mL) [illegible]olution was added to each well and incubated till the time [illegible]urple colou[illegible]develops in the well. Then, 100 µl of stop-p[illegible]g solutio[illegible](50% dimethyl formamide and 10% sodium dodec[illegible]ulphate) was added to stop the reaction, which [illegible]olves the purple formazan crystals. The plates were covered with aluminium foil and kept at 37°C incubator for 2 hrs for the complete dissolution of purple coloured formazan crystals. The amount of formazan crystals formed is directly proportional to the number of viable cells present in the well. The absorbance was measured using an ELISA plate reader (Tecan infinite M 200 pro, Tecan Austria GmbH, Grödig, Austria) at 570 nm. The percentage of cytotoxicity was defined as ([absorbance of treated cells]/[absorbance of control cell] ×100).

In vivo efficacy studies

The study was approved by the "committee for the purpose of control and supervision of experiments on animals" (CPCSEA, Government of India, Animal welfare division, Reg.No. 1994/GO/ReBi/S/17/CPCSEA) and all experiments were performed following institutional and national guidelines and regulations of the CPCSEA. The in vivo activity of the ST06-AgNPs was tested using tumour induced mouse model (Swiss Albino) developed by intravenously injecting Ehrlich ascites carcinoma (EAC) cells (1×10^6 cells) to either of the hind legs of mice. After tumours had developed to a size of ≃ 200 mm^3, animals were segregated (n=5) in a manner to equalize the mean tumor diameter among the

groups. Tumor bearing mice were divided into four experimental groups (ST06, ST06-AgNPs, blank AgNPs and control without drug treatment) and subjected to 15 doses of 5 mg/kg of body weight of ST06 and ST06-AgNPs intraperitoneally (i.p) every alternate day. The experiment was repeated three times with 5 animals each per group to a total number of n=15. Changes in the tumour size and body weight were observed for 30 days from the day of treatment. The width, length, and height of tumors were measured using a digital calliper. Tumor volume was calculated using the formula V = (L x W x W)/2, where V is tumor volume, W is tumor width, L is tumor length.

Western blot analysis

Tumor tissues (100 mg) from the three groups (tumor-bearing control without drug treatment, AgNPs treated, ST06 treated, ST06-AgNPs treatment) were minced and lysed in 500 µl cell lysis buffer for 30 mins, sonicated and centrifuged at 12,000 rpm for 15 mins at 4°C. The supernatant was collected and protein concentrations were determined by Bradford assay. Samples were subjected to 10% sodium dodecyl sulphate polyacrylamide gel electrophoresis (SDS-PAGE) and the resolved proteins were transferred to polyvinylidene difluoride (PVDF) membrane (Biorad, USA) by semi-dry transfer method (Transblot-Turbo blotting system, Biorad, USA). The membranes were blocked with 5% non-fat dried milk in Tris-buffered saline containing 0.1% Tween 20 (TBST) for 1 hr at room temperature, washed three times with TBST and incubated with primary antibody (Bcl-2, caspase 9, 3, PARP1) for 2 hrs at room temperature followed by respective secondary antibodies labelled with biotin. The antibodies were purchased from Santa Cruz Biotechnology Santa Cruz, CA and Cell Signalling Technology, Beverly, MA. After washing three times with TBST the membranes were incubated with streptavidin-horseradish peroxidase conjugate for 1 hr at room temperature. The antibody hybridized membrane was developed using chemiluminescence reagent (Clarity Western ECL blotting substrate, Biorad, USA). The blot images were captured using Syngene G: Box gel doc system and protein image quantification were done using GelQuant. Net, BiochemLab solutions.

Drug toxicity assessment

EAC tumor-induced mice were treated with ST06 and ST06-AgNPs for 30 days, after which the drug toxicity evaluation was carried out. Blood samples were collected from three animals from each group and the serum was separated. Drug toxicity biomarkers such as aspartate aminotransferase (AST), alanine aminotransferase (ALT) and urea were estimated according to the method described by ALT/AST/urea activity assay kit (Abcam, India).

Histological analysis of tumour tissues

H & E staining of the tumor and organs were performed by fixing the tissues in formalin. The tissues were then embedded in paraffin and the tissue blocks were sectioned into 5 mm thickness. For histological staining, the tissue slices were deparaffinized in xylene for 5 mins, dehydrated in ethanol gradient (100%, 70%, 50%, 30%) followed by washing with running water and incubation in hematoxylin for 5 min. The slides were then subjected to acid-alcohol wash (1% HCl in 70% of C_2H_5OH) and then kept in 2% sodium bicarbonate solution for 1 min, followed by washing with running water. It was then incubated in eosin for 30 seconds. The slides with the tissues were dehydrated in a solution of graded ethanol (70%, 100%) followed by xylene incubation for 5 min. The slides were then fixed using DPX mountant and allowed to dry for observation under the microscope.

Statistical analysis

All values in this study were presented as mean ± SE of at least 3 independent experiments. Two-way ANOVA for significance testing was used for multiple group analysis and Student's t-tests were used for two-group comparison. p-value ≤0.05 was considered as significant. The p-value was represented as * for p-value <0.05, ** for p<0.01, *** for p<0.001, **** for p-value <0.0001.

Results

Characterisation of ST06-AgNPs

The hydrodynamic diameter of ST06-AgNPs, as determined using DLS, was 74±0.52 nm with a low polydispersity index (PDI) of 0.202 (Figure 1A), indicating the formation of monodispersed nanoparticles. The Zeta potential of ST06-AgNPs was −35.3 mV. The observed high negative surface charge indicates the formation of stable nanoparticles (Figure 1B). The absorbance of the silver nanoparticles solutions was measured on a UV-Visible spectrometer. The AgNPs and ST06-AgNPs showed a characteristic silver plasmon band at 410 nm (Figure 1C and D). The average particle diameter, as analysed by TEM, was about 50–100 nm (Figure 2A). Elemental analysis by EDX presented a strong peak for silver at about 3 keV indicating that silver is the basic constituent element (Figure 2B). The FTIR spectra (Figure 2C) showed absorption

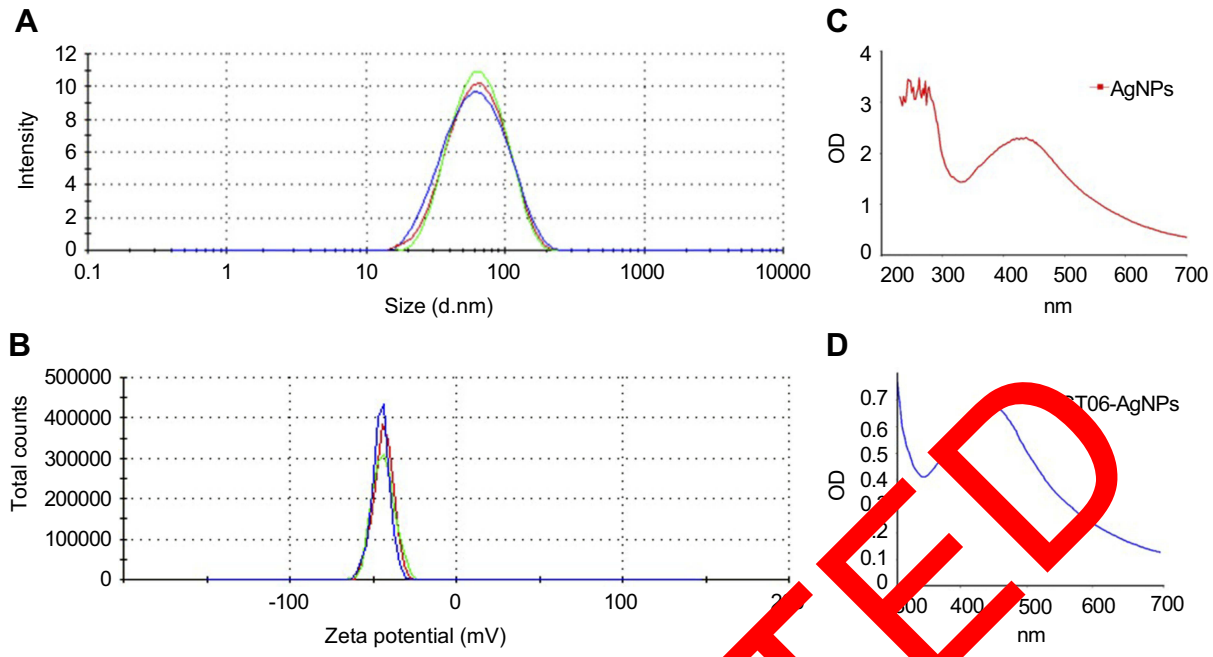

Figure 1 Characterization of ST06-AgNPs.
Notes: Particle size distribution of ST06-AgNPs by dynamic light scattering (DLS) (**A**) Zeta P[illegible] distribution o[illegible]T06-AgNPs (**B**) UV-vis spectra of the reaction mixture containing AgNPs (**C**) and ST06-AgNPs (**D**).

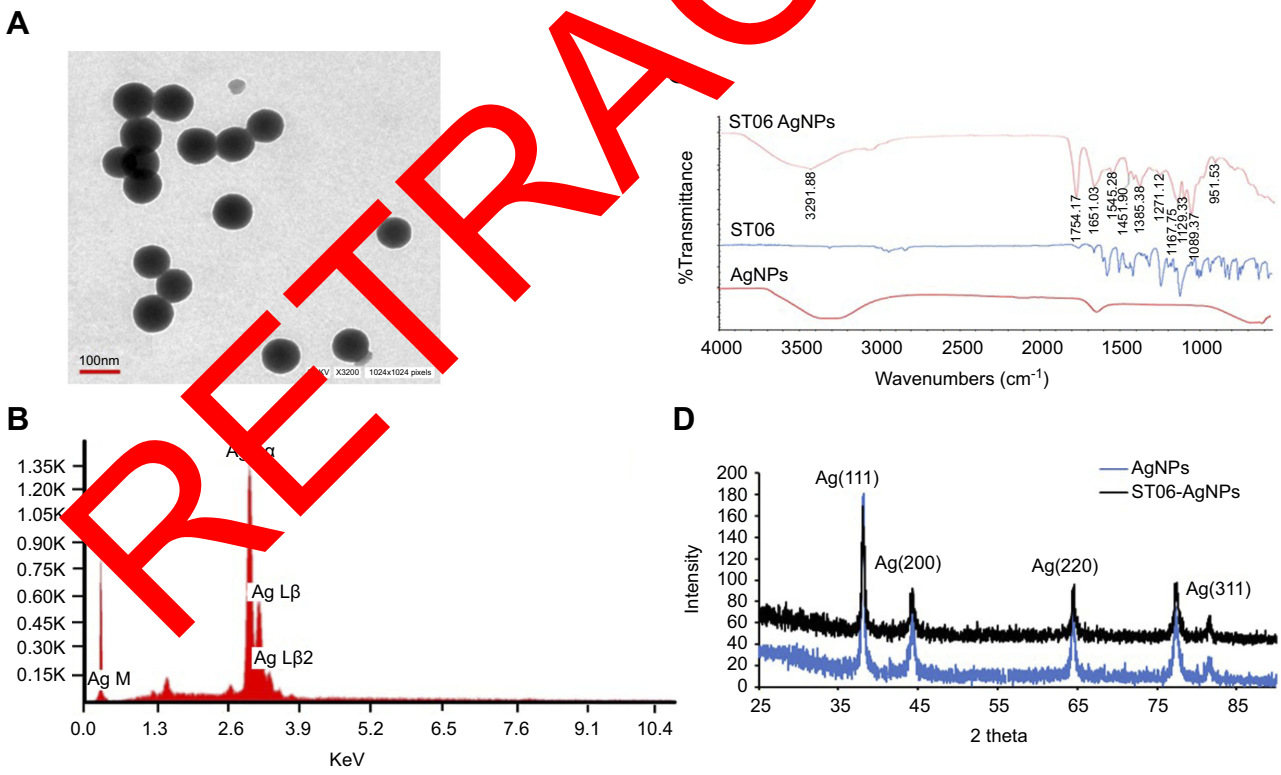

Figure 2 Size distribution of ST06-AgNPs as measured by transmission electron microscopy (TEM) (**A**) Energy dispersive X-ray spectrum of synthesised ST06-AgNPs (**B**) Fourier Transform Infrared spectroscopy of AgNPs, ST06, ST06-AgNPs (**C**) X-ray diffraction pattern of AgNPs and ST06-AgNPs (**D**).

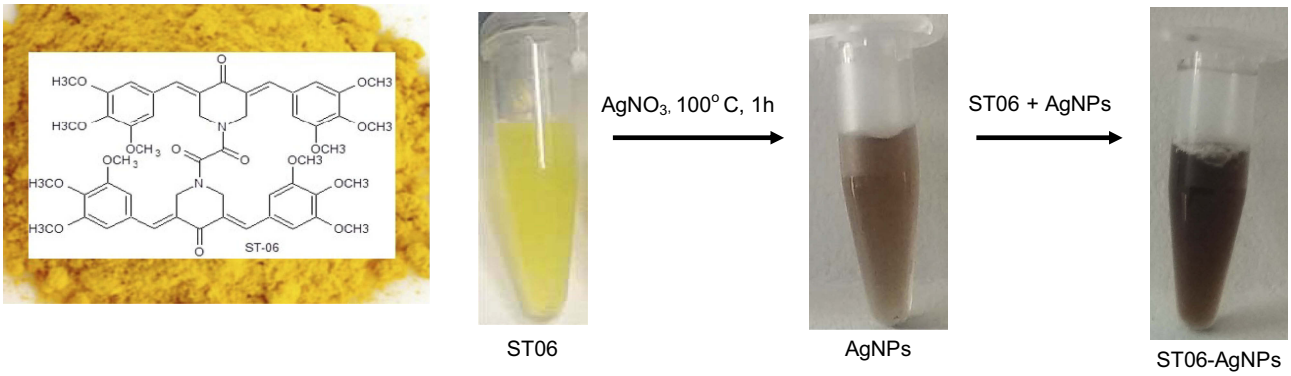

Figure 3 Green synthesis of ST06-AgNPs.
Notes: Green synthesis of ST06-AgNPs. Reduction of $AgNO_3$ to AgNPs with ST06 and synthesis of ST06 adsorbed AgNPs.

peaks from 3291 cm^{-1} to 612 cm^{-1}. The peak at 1651 cm^{-1} represents the carbonyl group (C=O) while the absorption peaks at 1271–1385 cm^{-1} correspond to amide groups. Stretching vibration at 3291cm^{-1} indicate N-H stretching and peak at 1271 cm^{-1} and 1089 cm^{-1} represents -OH and C-O-H stretching. The peak at 1545 cm^{-1} and 612 assigned to N-O stretching and aromatic C-H vibrations. Thus, from the FTIR spectra, it can be inferred that the synthesised ST06-AgNPs have been primarily functionalized by ST06, which may be responsible for efficient capping and stability of the nanoparticle. Moreover, a structure-activity relationship study against different cancer cell lines revealed that majority of the anti-cancer molecules contained functional groups like OH, R_2NH, R_3N, RCOR, ROR.[34,35] Hence, the FTIR results suggest that the synthesised nanoparticles are stabilized and functionalised preferentially to demonstrate its anti-cancer effects.

The crystalline nature of AgNPs and ST06-AgNPs was verified by XRD. The XRD pattern was recorded at 25°- 90° at two angles. High-intensity peaks from XRD patterns were observed around 37°, 44°, 64° and 84° corresponding to diffraction faces of silver. The XRD peak at 37°37°, 44°, 64°, and 84° represented the Bragg reflection corresponding to (111), (200), (220) and 311 planes (Figure 2D).

Effects of ST06 and ST06-AgNPs on HeLa cell lines

ST06-AgNPs were tested for their inhibitory effects on HeLa cervical cancer cell line. Cytotoxicity analysis by MTT assay showed a dose dependent decrease in the viability of cancer cells (Figure 4). About 50% of the cells were killed at a concentration of 1 µM of ST06 (P<0.01) and 1 µM of ST06-AgNPs (P<0.01). AgNPs showed a significant reduction at 2 µM (P<0.01). The anti-cancer activity of green synthesised AgNPs on HeLa cells has been reported earlier.[19,36] In a study, green synthesised AgNPs exhibited anti-cancer activity at a concentration of 5 and 2 µg/ml on HeLa cells.[19] Manivasagan et al showed IC50 value to be 200 ug/ml of AgNPs against HeLa cancer cells.[36] But the effective doses used in these studies were considerably higher than those observed in the present study (IC_{50}, 1 µM, Figure 4).

Effects of ST06 and ST06-AgNPs on EAC tumor induced mice

EAC tumor induced mice were divided into four experimental groups (n=15, ST06, blank AgNPs, ST06-AgNPs, untreated control) and subjected to 15 doses of ST06, ST06-AgNPs, blank AgNPs (5 mg/kg body weight) separately through intraperitoneal (i.p) route. At the end of treatment, tumor from each mouse from all the four groups was excised and weighed. The average tumor weight was 4.24 g for control, 3.23 g for AgNPs, 2.68 g for ST06, and 0.992 g for ST06-AgNPs (Figure 5A). The animals were segregated such that the initial tumor volume in all the groups was similar. The average initial tumor volume at the start of the experiment was 0.23 cm^3 for the control (untreated), 0.26 cm^3 for AgNPs, 0.25 cm^3 for ST06 and 0.25 cm^3 for ST06-AgNPs treated group. After 30 days of treatment, the average tumor volume of ST06-AgNPs decreased significantly compared to the treatment with AgNPs, ST06 and control groups (Figure 5B). The average tumor volume in mice after treatment was 3.6 cm^3 for control group, 2.2 cm^3 for AgNPs, 1.8 cm^3 for ST06, and 0.66 cm^3 for the ST06-AgNPs (Figure 5C). Statistical analysis by two-way ANOVA showed that the tumor volume of the treatment groups were significantly reduced on comparison with the untreated controls; ST06-AgNPs (P=0.0015), blank AgNPs (P=0.05) and ST06 treatment groups (P=0.01). These results clearly revealed that ST06-AgNPs inhibited the tumor

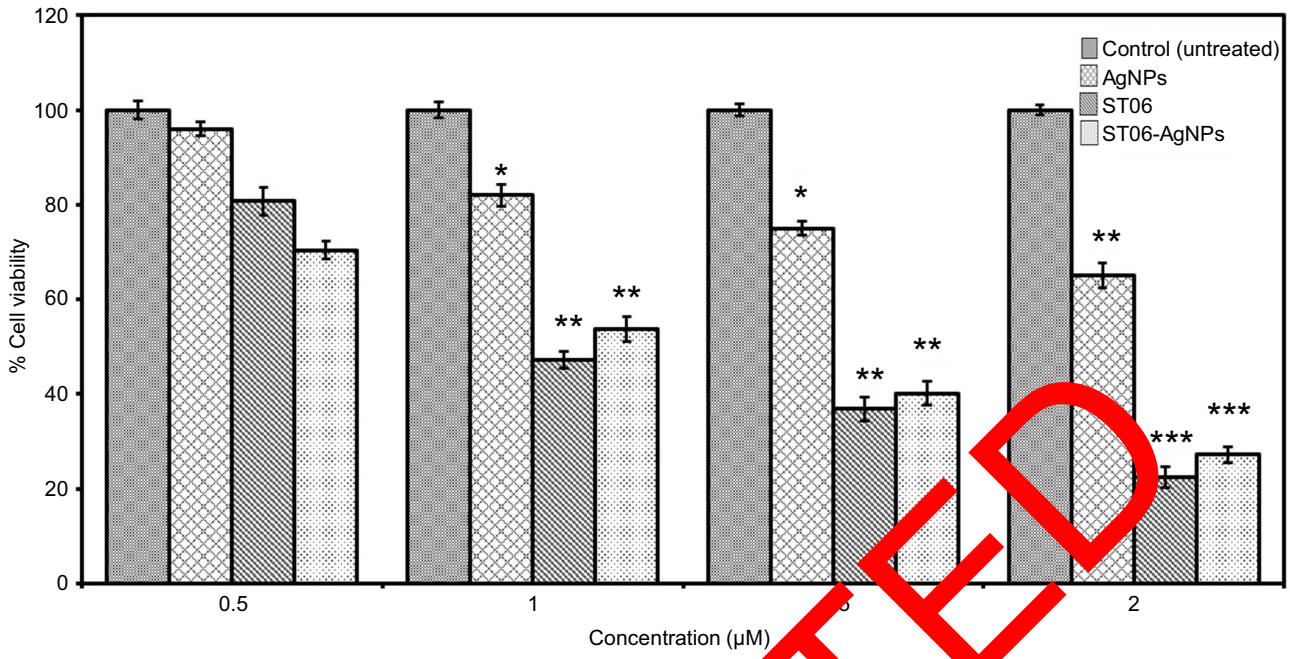

Figure 4 Cytotoxicity effect by MTT assay of AgNPs, ST06 and ST06-AgNPs on HeLa cells.
Notes: HeLa cells were exposed to different concentrations of AgNPs, ST06 and ST06-AgNPs for 48 hrs and its effect on cell viability analyzed by MTT assay. This experiment was repeated thrice, and bars represent SE *P<0.05, **P<0.01, ***P<0.001 compared with the untreated control.

growth much more efficiently, compared to the free ST06 and AgNPs treatment groups. The average initial body weight of animals at the start of the experiment was 26.48 g for the control, 26.24 g for ST06, 26.2 for AgNPs and 26.38 g for ST06-AgNPs treated groups (Figure 5D). The body weight changes in all the four groups were found to be similar towards the end of the experiment. Based on these results, we infer that ST06-AgNPs given at a concentration of 5 mg/kg intraperitoneally significantly inhibited the tumor growth in tumor-bearing animals, without affecting their body weight.

Effects of ST06 and ST06-AgNPs on the levels of bcl-2, caspase 3,9 and PARP

After treatment with ST06 and ST06-AgNPs, expression of the apoptosis-associated proteins in tumour tissues was investigated in order to understand the mechanism involved in tumor reduction. Results showed that the expression of parent caspase 9 decreased by 0.3 and 0.5-fold, respectively, in the ST06 and ST06-AgNPs treatment groups, compared to the control group. At the same time, the expression of cleaved caspase 9 increased by~2fold, whereas the expression of cleaved caspase 3 increased by ~4-fold in both the treatment groups. Meanwhile, cleaved PARP expression increased by ~0.44 -fold in ST06-AgNPs, whereas the Bcl-2 expression decreased in both the groups by ~0.15 fold (Figure 6). These results suggest activation of the caspases involved in the intrinsic pathway, along with the cleavage of parent PARP in treated tumor tissues.

Toxicity assessment

After 30 days of treatment with ST06 and ST06-AgNPs the serum samples were collected from the mice and analysed for alkaline aminotransferase (ALT), aspartate aminotransferase (AST) and urea contents. The results shown in Figure 7 reveal that serum AST and ALT levels were within the normal range in both the treatment groups (AST<100 U/L and ALT <60 U/L), whereas in case of urea, the levels were slightly higher than the normal range (Urea<35 mM/L).

Histological analysis of tumor tissues and organs

Tumor tissues from both the experimental groups and control group were fixed with formalin, embedded in paraffin and sectioned. The H&E-stained sections of major organs, such as liver, spleen and kidney, were analysed and the histological results compared with the results of the biochemical analysis. No severe abnormalities were identified in both the treatment groups. The sections of organs were observed for changes such as necrosis, hypertrophy, hyperplasia,

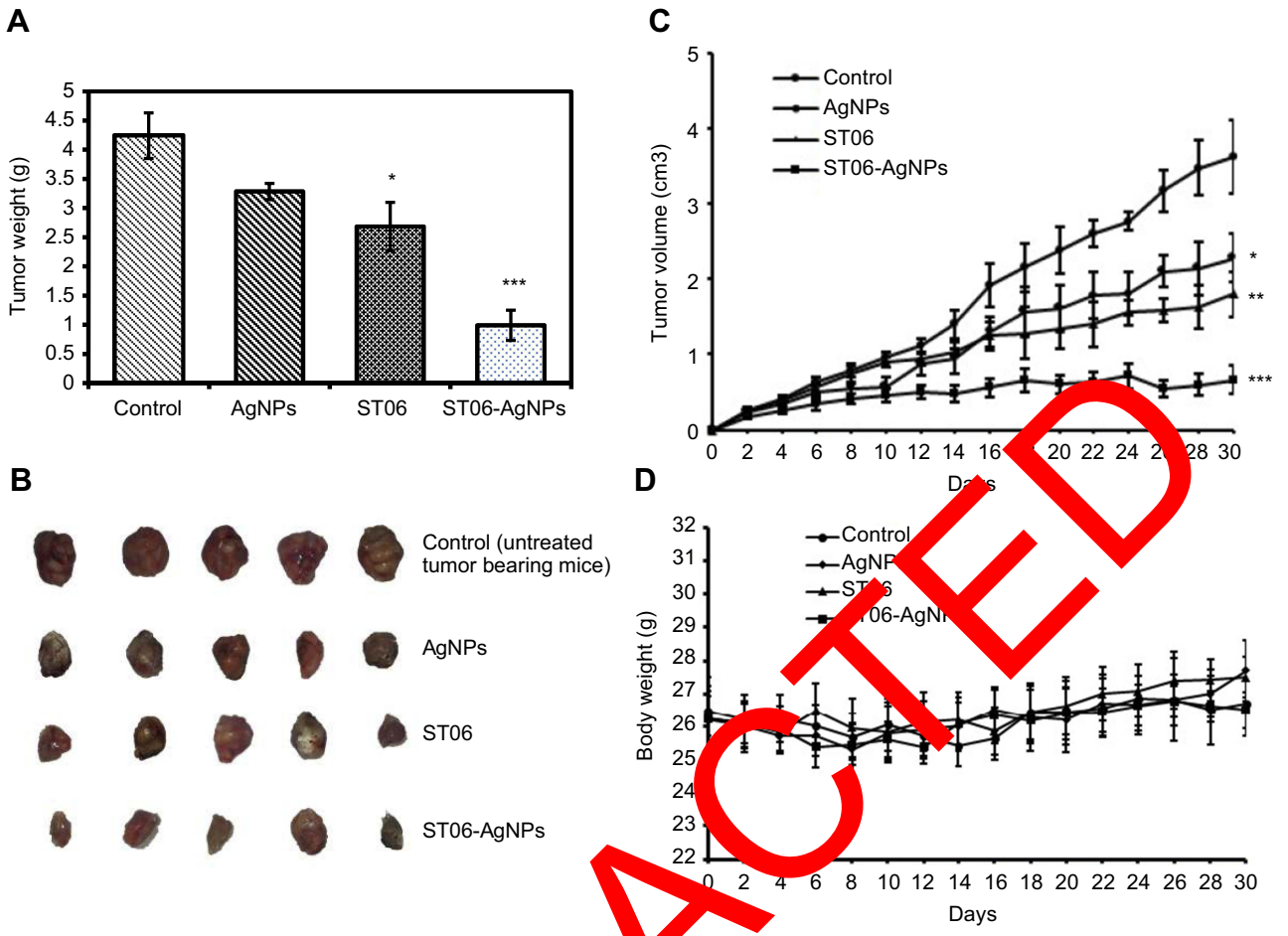

Figure 5 The in vivo effects of AgNPs, ST06 and ST06-AgNPs in EAC tumor bearing mice.
Notes: Individual tumor weight of mice after 30 days of treatment (**A**) Images of tumors removed from mice in each group after treatment (**B**) Growth curve of EAC tumors in each group (**C**) Individual body weight of mice after treatment. Each value represents mean ±SE from fifteen mice *P<0.05, **P<0.01,*** P<0.001.

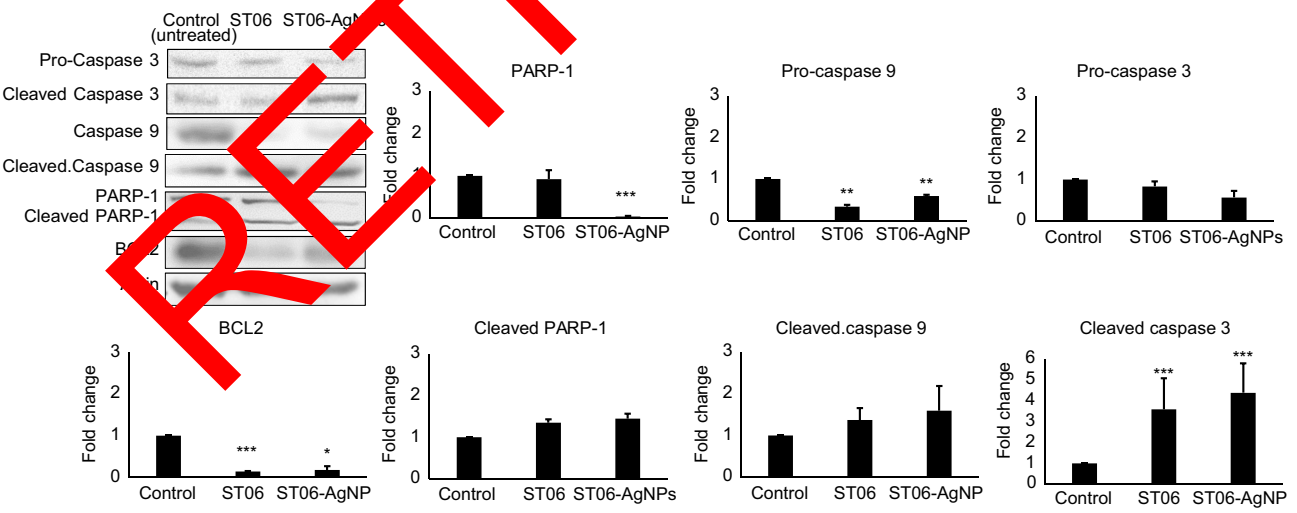

Figure 6 Apoptosis protein expression in tumor tissues.
Notes: The cell lysates were subjected to SDS-PAGE and blotted with Caspase 3, Cleaved caspase 3, Caspase 9, Cleaved caspase 9, PARP-1, Cleaved PARP-1 and BCL2 antibodies.The data are representative of 3 experiments. Each value represents mean ±SE of three experiments. *P<0.05, **P<0.01,*** P<0.001.

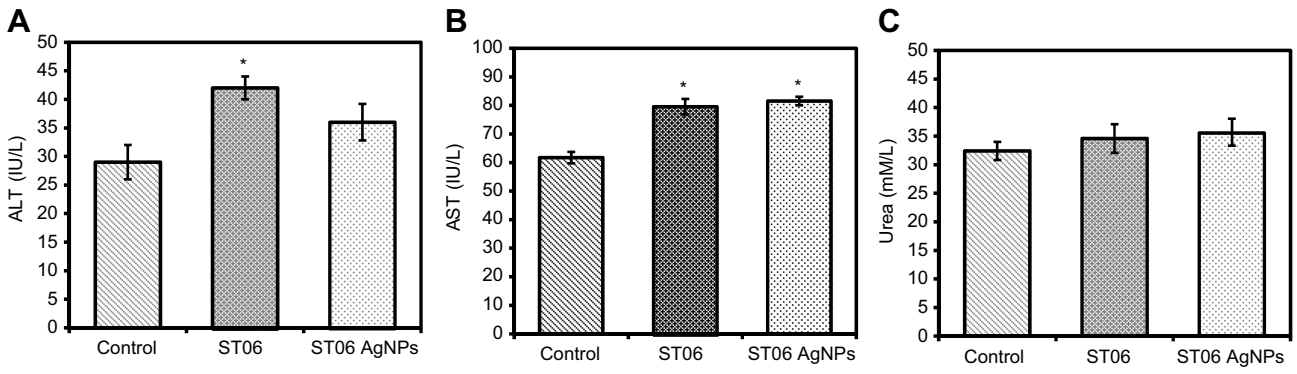

Figure 7 Toxicity assessment of ST06-AgNPs.
Notes: Plasma levels of AST (**A**) ALT (**B**) and Urea (**C**) after 30 days of treatment with ST06 and ST06-AgNPs. Each value represents mean ±SD of three experiments. *P<0.05, **P<0.01,***P<0.001****P<0.0001 compared with the untreated control.
Abbreviations: AST, aspartate aminotransferase; ALT, alanine aminotransferase.

pigmentation, steatoses in the liver; loss of germinal centers, enlargement of the red and white pulp of spleen; vacuolation of tubules in the kidney. Treatment with ST06 and ST06-AgNPs significantly improved the morphological/histopathological conditions, compared to the control group (Figure 8). Further, the H & E stained sections of tumor tissues in the treatment groups exhibited a significant reduction in the number of blood vessel formation, [illegible] pared to the controls (Figure 8).

Discussion

AgNPs ha[illegible] been wi[illegible]ly recognised for their anti-bacteria[illegible]–3] anti-fungal,[illegible] anti-viral,[32,42] and anti-inflammatory effe[illegible]ts.[43,44] Recently, AgNPs synthesised using plants, bacteria and fungi products have been reported to have a wide range of applications in cancer treatment and biomedical field.[45–47] Several plants and microbial based AgNPs have been shown to exhibit enhanced cytotoxicity on a variety of adherent and non-adherent cancer cell lines.[48] Besides, the in vivo anti-

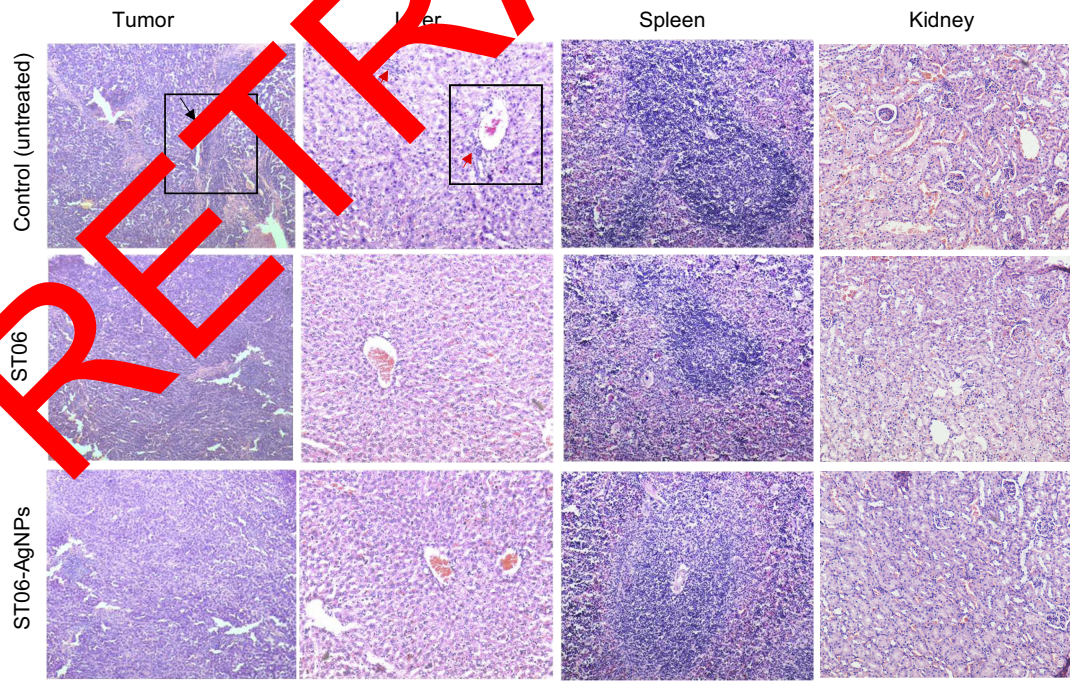

Figure 8 The micrographs of H&E-stained sections of the main organs and tumors after treatment with ST06 and ST06-AgNPs.
Notes: Hematoxylin and eosin-stained tumor, liver, spleen and kidney tissue after ST06 and ST06-AgNPs treatment of mice (treatment every second day for 30 days). Angiogenesis (black arrow), hyperplasia (red arrow).

tumorigenic potential of AgNPs has been demonstrated in Dalton's lymphoma tumor-bearing mice[29] and L5178Y-R tumor bearing mice[49] models.

Curcumin, from *Curcuma longa*, is well recognized for its chemo preventive and antitumor properties, however, its instability and poor bioavailability are the major problems in its therapeutic application.[1,50] Modifications or substitutions on the aromatic ring of curcumin have been reported to alter the metabolic stability and cytotoxicity[51] of the parent molecule. Several compounds containing 4-fluro, 4-chloro, 4-hydroxy or 3,4,5 trimethoxy substitutions were found to be potent inhibitors of several cancer cell types at sub micromolar concentrations[9]. Furthermore, a large number of curcumin based nano-formulations have been reported to enhance curcumin therapeutic efficacy.[52] Moreover, curcumin modified AgNPs (Cur-AgNPs) were shown to significantly inhibit respiratory syncytial virus;[32] reduce replication of HIV;[53] exhibit antibacterial activity;[54] and improve the therapeutic efficacy of collagen for biomedical applications[55] In the present study, we report the synthesis, characterisation and evaluation of cytotoxic activity of ST06 (a curcumin derivative) and ST06 loaded on to AgNPs (ST06-AgNPs) on human cervical cancer cells (HeLa) and also in EAC tumor-bearing mice model. The results revealed that ST06-AgNPs exhibit significantly higher anticancer activity, as compared to free ST06 or AgNPs.

Earlier studies have proposed different mechanisms such as apoptosis, induction of reactive oxygen species (ROS) and silver ion release, for the anti-cancer potential of AgNPs.[24] The cascade of events in the execution of apoptosis involves caspase and Bcl-2 families of proteins. It has been reported that down regulation of Bcl-2 leads to release of cytochrome c followed by activation of caspase 9, 3 and cleavage of PARP which eventually leads to apoptosis.[56] In this study, the protein expression analysis of tumor tissues revealed a significant decrease in the expression of Bcl-2 whereas the expression of pro-apoptotic proteins caspase-9, and 3 and cleavage of PARP1 was upregulated in both the treatment groups. These findings suggest that ST06 and ST06-AgNPs inhibits the tumor growth by induction of mitochondria-mediated caspases dependent apoptosis.

Although, both ST06 and ST06-AgNPs showed inhibitory effects on the tumor growth, ST06 adsorbed on to AgNPs (ST06-AgNPs) exhibited greater efficacy than the free drug or AgNPs, because of adsorption of the drug to relatively larger surface area of nanoparticles, which might have enhanced the dissolution rate of the drug by Van der Waals forces, and hydrogen bonds.[57] This is well supported by the earlier studies, which have shown that adsorption of drugs and antibiotics to AgNPs significantly enhanced their bioactivity, compared to free drug.[33,58] Further, AgNPs though have been widely employed as drug carriers in the biomedical field but only limited studies have been carried out to assess their toxic effects. The biochemical and histological analyses in the present study indicated that both ST06 and ST06-AgNPs exhibited no significant toxic effects in the animals at the given dose (5 mg/Kg). This is in agreement with earlier studies, which have shown that the toxicity of the AgNPs depends upon the particles size and their injected dose. It has been reported that small size AgNPs cause multi organ toxicity such as liver and kidney, toxicity at high doses (13–21 mg/kg), however lower doses exhibited negligible toxic effects.[59,60] And the H & E sections of tumor tissues exhibited a significant reduction in the number of blood vessel formation in the ST06 and ST06-AgNPs treatment groups. Compared to the controls, it is inferred that both the treatments might have impaired the angiogenesis in tumors, which in turn could have resulted in inhibition of the tumor growth and progression. This is well supported by the earlier studies, which have shown that AgNPs effectively impede new blood vessels formation in bovine retinal endothelial cells[28] and in chick chorioalantoic membrane.[61] Taken together, these results suggest that the synthesised nanoparticles (ST06-AgNPs) possess strong anti-tumorigenic and anti-angiogenic potential against EAC tumors.

Acknowledgments

The authors would like to acknowledge the funding provided by the Department of Biotechnology (DBT, New Delhi) under the grant scheme of BioCare Women Scientist. The authors thank the Institute of Bioinformatics and Applied Biotechnology (IBAB) for providing the animal house facilities for conducting our experiments.

Disclosure

The authors report no conflicts of interest in this work.

References

1. Garcea G, Jones DJL, Singh R, et al. Detection of curcumin and its metabolites in hepatic tissue and portal blood of patients following oral administration. *Br J Cancer*. 2004;90(5):1011–1015. doi:10.1038/sj.bjc.6601623
2. Yang KY, Lin L-C, Tseng T-Y, Wang S-C, Tsai T-H. Oral bioavailability of curcumin in rat and the herbal analysis from Curcuma longa by LC-MS/MS. *J Chromatogr B Analyt Technol Biomed Life Sci*. 2007;853(1–2):183–189. doi:10.1016/j.jchromb.2007.03.010

3. Wei X, Du Z-Y, Zheng X, Cui X-X, Conney AH, Zhang K. Synthesis and evaluation of curcumin-related compounds for anticancer activity. *Eur J Med Chem*. 2012;53:235–245. doi:10.1016/j.ejmech.2012.04.005
4. Gafner S, Lee S-K, Cuendet M, et al. Biologic evaluation of curcumin and structural derivatives in cancer chemoprevention model systems. *Phytochemistry*. 2004;65(21):2849–2859. doi:10.1016/j.phytochem.2004.08.008
5. Li Q, Chen J, Luo S, Xu J, Huang Q, Liu T. Synthesis and assessment of the antioxidant and antitumor properties of asymmetric curcumin analogues. *Eur J Med Chem*. 2015;93:461–469. doi:10.1016/j.ejmech.2015.02.005
6. Brown A, Shi Q, Moore TW, et al. Monocarbonyl curcumin analogues: heterocyclic pleiotropic kinase inhibitors that mediate anticancer properties. *J Med Chem*. 2013;56(9):3456–3466. doi:10.1021/jm4002692
7. Paul NK, Jha M, Bhullar KS, Rupasinghe HPV, Balzarini J, Jha A. All trans 1-(3-arylacryloyl)-3,5-bis(pyridin-4-ylmethylene)piperidin-4-ones as curcumin-inspired antineoplastics. *Eur J Med Chem*. 2014;87:461–470. doi:10.1016/j.ejmech.2014.09.090
8. Samaan N, Zhong Q, Fernandez J, et al. Design, synthesis, and evaluation of novel heteroaromatic analogs of curcumin as anti-cancer agents. *Eur J Med Chem*. 2014;75:123–131. doi:10.1016/j.ejmech.2014.01.041
9. Yahaira S, Swagatika D, Umashankar D, et al. Novel 3,5-bis-(arylidene)-4-oxo-1-piperidinyl dimers: structure—activity relationships and potent antileukemic and antilymphoma cytotoxicity. *Eur J Med Chem*. 2014;77:315–322. doi:10.1016/j.ejmech.2014.03.009
10. Pathak L, Kanwal A, Agrawal Y. Curcumin loaded self-assembled lipid-biopolymer nanoparticles for functional food applications. *J Food Sci Technol*. 2015;52(10):6143–6156. doi:10.1007/s13197-015-1742-2
11. Hembram KC, Kumar R, Kandha L, Parhi PK, Kundu CN, Bindhani BK. Therapeutic prospective of plant-induced silver nanoparticles: application as antimicrobial and anticancer agent. *Artif Cells Nanomed Biotechnol*. 2018;46(sup3):S38–S51. doi:10.1080/21691401.2018.1489262
12. Ovais M, Khalil AT, Raza A, et al. Green synthesis of silver nanoparticles via plant extracts: beginning a new era in cancer theranostics. *Nanomedicine (Lond)*. 2016;11(23):3157–3177. doi:10.2217/nnm-2016-0279
13. Yadi M, Mostafavi E, Saleh B, et al. Current developments in green synthesis of metallic nanoparticles using plant extracts: a review. *Artif Cells Nanomed Biotechnol*. 2018;46(sup3):S336–S343. doi:10.1080/21691401.2018.1492931
14. Kayalvizhi T, Ravikumar S, Velayutham P. Green synthesis of metallic silver nanoparticles using *Couroupita guianensis* Aubl. fruit extracts and evaluation of their antibacterial, larvicidal, and anticancer activity. *J Environ Eng*. 2016;142(9):1–10. doi:10.1061/(ASCE)EE.1943-7870.0001063
15. Jang SJ, Yang IJ, Choi CO, Kim KM, Shin HM. In-vitro anticancer activity of green synthesized silver nanoparticles on MCF-7 human breast cancer cells. *Mater Sci Eng C Mater Biol Appl*. 2016;68:430–435. doi:10.1016/j.msec.2016.03.101
16. Castro-Aceituno V, Ahn S, Simu SY, et al. Anticancer activity of silver nanoparticles from *Panax ginseng* fresh leaves in human cancer cells. *Biomed Pharmacother*. 2016;84:158–165. doi:10.1016/j.biopha.2016.09.016
17. Kummara S, Patil MB, Uriah T. Synthesis, characterization, biocompatible and anticancer activity of green and chemically synthesized silver nanoparticles - A comparative study. *Biomed Pharmacother*. 2016;84:10–21. doi:10.1016/j.biopha.2016.09.003
18. Banerjee PP, Bandyopadhyay A, Harsha SN, et al. Mentha arvensis (Linn.)-mediated green silver nanoparticles trigger caspase 9-dependent cell death in MCF7 and MDA-MB-231 cells. *Breast Cancer (Dove Med Press)*. 2017;9:265–278. doi:10.2147/BCTT.S130952
19. Singh H, Du J, Yi T-H. Green and rapid synthesis of silver nanoparticles using Borago officinalis leaf extract: anticancer and antibacterial activities. *Artif Cells Nanomed Biotechnol*. 2017;45(7):1310–1316. doi:10.1080/21691401.2016.1228663
20. Wang C, Mathiyalagan R, Kim YJ, et al. Rapid green synthesis of silver and gold nanoparticles using Dendropanax morbifera leaf extract and their anticancer activities. *Int J Nanomedicine*. 2016;11:3691–3701. doi:10.2147/IJN.S97181
21. Jeyaraj M, Sathishkumar G, Sivanandhan G, et al. Biogenic silver nanoparticles for cancer treatment: an experimental report. *Colloids Surf B Biointerfaces*. 2013;106:86–92. doi:10.1016/j.colsurfb.2013.01.027
22. Gengan RM, Anand K, Phulukdaree A, Chuturgoon A. A549 lung cell line activity of biosynthesized silver nanoparticles using Albizia adianthifolia leaf. *Colloids Surf B Biointerfaces*. 2013;105(4):87–91. doi:10.1016/j.colsurfb.2012.12.044
23. Sanpui P, Chattopadhyay A, Ghosh SS. Induction of apoptosis in cancer cells at low silver nanoparticle concentrations using chitosan nanocarrier. *ACS Appl Mater Interfaces*. 2011;3(2):218–228. doi:10.1021/am100840c
24. Jeyaraj M, Rajesh M, Arun R, et al. An investigation on the cytotoxicity and caspase-mediated apoptotic effect of biologically synthesized silver nanoparticles using Podophyllum hexandrum on human cervical carcinoma cells. *Colloids Surf B Biointerfaces*. 2013;102:708–717. doi:10.1016/j.colsurfb.2012.09.042
25. Hsin YH, Chen CF, Huang S, Shih T-S, Lai P-S, Chueh PJ. The apoptotic effect of nanosilver is mediated by a ROS- and JNK-dependent mechanism involving the mitochondrial pathway in NIH3T3 cells. *Toxicol Lett*. 2008;179(3):130–139. doi:10.1016/j.toxlet.2008.04.015
26. AshaRani PV, Low Kah Mun G, Hande MP, Valiyaveettil S. Cytotoxicity and genotoxicity of silver nanoparticles in human cells. *ACS Nano*. 2009;3(2):279–290. doi:10.1021/nn800596w
27. Kalishwaralal K, Banumathi E, Ram Kumar Pandian S, et al. Silver nanoparticles inhibit VEGF induced cell proliferation and migration in bovine retinal endothelial cells. *Colloids Surf B Biointerfaces*. 2009;73(1):51–57. doi:10.1016/j.colsurfb.2009.04.025
28. Gurunathan S, Lee K-J, Kalishwaralal K, Sheikpranbabu S, Vaidyanathan R, Eom SH. Antiangiogenic properties of silver nanoparticles. *Biomaterials*. 2009;30(31):6341–6350. doi:10.1016/j.biomaterials.2009.08.008
29. Antony JJ, Sithika MAA, Joseph TA, et al. In vivo antitumor activity of biosynthesized silver nanoparticles using Ficus religiosa as a nanofactory in DAL induced mice model. *Colloids Surf B Biointerfaces*. 2013;108:185–190. doi:10.1016/j.colsurfb.2013.02.041
30. Sriram MI, Kanth SBM, Kalishwaralal K, Gurunathan S. Antitumor activity of silver nanoparticles in Dalton's lymphoma ascites tumor model. *Int J Nanomedicine*. 2010;5:753–762. doi:10.2147/IJN.S11727
31. Jacob JA, Shanmugam A. Silver nanoparticles provoke apoptosis of Dalton's ascites lymphoma in vivo by mitochondria dependent and independent pathways. *Colloids Surf B Biointerfaces*. 2015;136:1011–1016. doi:10.1016/j.colsurfb.2015.11.004
32. Yang XX, Li CM, Huang CZ. Curcumin modified silver nanoparticles for highly efficient inhibition of respiratory syncytial virus infection. *Nanoscale*. 2016;8(5):3040–3048. doi:10.1039/c5nr07918g
33. Ahmad A, Wei Y, Syed F, et al. Isatis tinctoria mediated synthesis of amphotericin B-bound silver nanoparticles with enhanced photoinduced antileishmanial activity: a novel green approach. *J Photochem Photobiol B*. 2016;161:17–24. doi:10.1016/j.jphotobiol.2016.05.003
34. Singh H, Kumar R, Singh S, Chaudhary K, Gautam A, Raghava GPS. Prediction of anticancer molecules using hybrid model developed on molecules screened against NCI-60 cancer cell lines. *BMC Cancer*. 2016;16:77. doi:10.1186/s12885-016-2082-y
35. Fuchs JR. Structure-activity relationship studies of curcumin analogues. *Bioorg Med Chem Lett*. 2009;19(7):2065–2069.

36. Manivasagan P, Venkatesan J, Senthilkumar K, Sivakumar K, Kim SK. Biosynthesis, antimicrobial and cytotoxic effect of silver nanoparticles using a novel Nocardiopsis sp. MBRC-1. *Biomed Res Int*. 2013;287638. doi:10.1155/2013/287638
37. Kheybari S, Samadi N, Hosseini SV, Fazeli A, Fazeli MR. Synthesis and antimicrobial effects of silver nanoparticles produced by chemical reduction method. *Daru*. 2010;18(3):168–172.
38. Franci G, Falanga A, Galdiero S, et al. Silver nanoparticles as potential antibacterial agents. *Molecules*. 2015;20(5):8856–8874. doi:10.3390/molecules20058856
39. Okafor F, Janen A, Kukhtareva T, Edwards V, Curley M. Green synthesis of silver nanoparticles, their characterization, application and antibacterial activity. *Int J Environ Res Public Health*. 2013;10 (10):5221–5238. doi:10.3390/ijerph10105221
40. Kim SW, Jung JH, Lamsal K, Kim YS, Min JS, Lee YS. Antifungal effects of silver nanoparticles (AgNPs) against various plant pathogenic fungi. *Mycobiology*. 2012;40(1):53–58. doi:10.5941/MYCO.2012.40.1.053
41. Bocate KP, Reis GF, de Souza PC, et al. Antifungal activity of silver nanoparticles and simvastatin against toxigenic species of Aspergillus. *Int J Food Microbiol*. 2018;291:79–86. doi:10.1016/j.ijfoodmicro.2018.11.012
42. Lara HH, Garza-Treviño EN, Ixtepan-Turrent L, Singh DK. Silver nanoparticles are broad-spectrum bactericidal and virucidal compounds. *J Nanobiotechnology*. 2011;3(9):30. doi:10.1186/1477-3155-9-30
43. Wong KKY, Cheung SOF, Huang L, et al. Further evidence of the anti-inflammatory effects of silver nanoparticles. *ChemMedChem*. 2009;4(7):1129–1135. doi:10.1002/cmdc.200900049
44. Alessandrini F, Vennemann A, Gschwendtner S, et al. Pro-inflammatory versus immunomodulatory effects of silver nanoparticles in the lung: the critical role of dose, size and surface modification. *Nanomaterials*. 2017;7(10). doi:10.3390/nano7120458.
45. Syed A, Saraswati S, Kundu GC, Ahmad A. Biological synthesis silver nanoparticles using the fungus Humicola sp. and evaluati of their cytoxicity using normal and cancer cell lines. *Spectrochim Acta A Mol Biomol Spectrosc*. 2013;114:144–147. doi:10.1016/j.saa.2013.05.030
46. Venugopal K, Ahmad H, Manikandan E, et al. Th impact o antic-ancer activity upon Beta vulgaris extract med d biosy silver nanoparticles (ag-NPs) against hum breas MCF-7), lung (A549) and pharynx (Hep-2) cancer ell lines. *Photochem Photobiol B*. 2017;173:99–107. doi:10. /j.jphotobiol.2 7.05.031
47. Shahnaz M, Lycias Joel E, Hasnain M . Nove en approach for synthesis of metallic nanoparticles an its biomedica plication. *Cnanom*. 2018;8(3):177–183. doi:10.217 2468187308666180 142158
48. Sunita P, Sivaraj R, Ven atesh R. anathi P, Rajiv P. Anticancer potential of green sy esized ilver nanoparticles: a review. *Int J Curr Res Rev*. 2015; 1539–2154
49. Lara-González JH, Gomez-Flores R, Tamez-Guerra P, Monreal-Cuevas E, Tamez-Guerra R, Rodríguez-Padilla C. In vivo antitumor activity of metal silver and silver nanoparticles in the L5178Y-R murine lymphoma model. *Br J Med Med Res*. 2013;3 (4):1308. doi:10.9734/BJMMR/2013/3108
50. Shehzad A, Wahid F, Lee YS. Curcumin in cancer chemoprevention: molecular targets, pharmacokinetics, bioavailability, and clinical trials. *Arch Pharm*. 2010;343(9):489–499. doi:10.1002/ardp.200900319
51. Sahu PK. Design, structure activity relationship, cytotoxicity and evaluation of antioxidant activity of curcumin derivatives/analogues. *Eur J Med Chem*. 2016;121:510–516. doi:10.1016/j.ejmech.2016.05.037
52. Naksuriya O, Okonogi S, Schiffelers RM, Hennink WE. Curcumin nanoformulations: a review of pharmaceutical properties and preclinical studies and clinical data related to cancer treatment. *Biomaterials*. 2014;35(10):3365–3383. doi:10.1016/j.biomat 2013.12.090
53. Sharma RK, Cwiklinski K, Aalinkeel R et al. I nomodulatory activities of curcumin-stabilized silv nanoparticles: fficacy as an antiretroviral therapeutic. *Immunol vest*. 2017;4):833–846. doi:10.1080/08820139.2017.13 908
54. Varaprasad K, Vimala K, R ndra S, Nara a Re y N, Venkata Subba Reddy G, Mohan aju K. F ication ver nanocomposite films impregnated th cu min for superior antibacterial applications. *J M er Sc ter Med* 2011;22(8):1863–1872. doi:10.1007/s10 -011-4369-
55. Srivatsan KV D ipandy N, Be S, et al. Effect of curcumin caged silv nanop le on collagen stabilization for biomedical applications. *Int J Biol acromol*. 2015;75:306–315. doi:10.1016/j.ijbi ac.2015.01.050
56. H upt S, Berger M, Goldberg Z, et al. Apoptosis - the p53 network. *Cell Sci*. 2003; 6:4077–4085. doi:10.1242/jcs.00739
57. L ne T, Burd C. Nanoparticle mediated non-covalent drug de ry. *Adv D g Deliv Rev*. 2013;65(5):607–621. doi:10.1016/j.addr.2 2
58. adhariya N, Khurana C, Chudasama B, Vala AK, Pandey OP. nhi of antibiotic adsorption on biocidal activities of silver nanoparticles. *IET Nanobiotechnol*. 2016;10(2):69–74. doi:10.1049/iet-nbt.2015.0005
59. Pani JP. Small size nanosilver multi organ toxicity: a higher dose negative response in in-vivo and in-vitro experimental application. *Bjstr*. 2017;1(4). doi:10.26717/BJSTR
60. Singh SP, Bhargava CS, Dubey V, Mishra A, Singh Y. Silver nanoparticles: biomedical applications, toxicity, and safety issues. *Int J Pharm Pharm Sci*. 2017;4(2):01–10.
61. Baharara J, Namvar F, Mousavi M, Ramezani T, Mohamad R. Anti-angiogenesis effect of biogenic silver nanoparticles synthesized using Saliva officinalis on chick chorioalantoic membrane (CAM). *Molecules*. 2014;19(9):13498–13508. doi:10.3390/molecules190913498

Supplementary materials

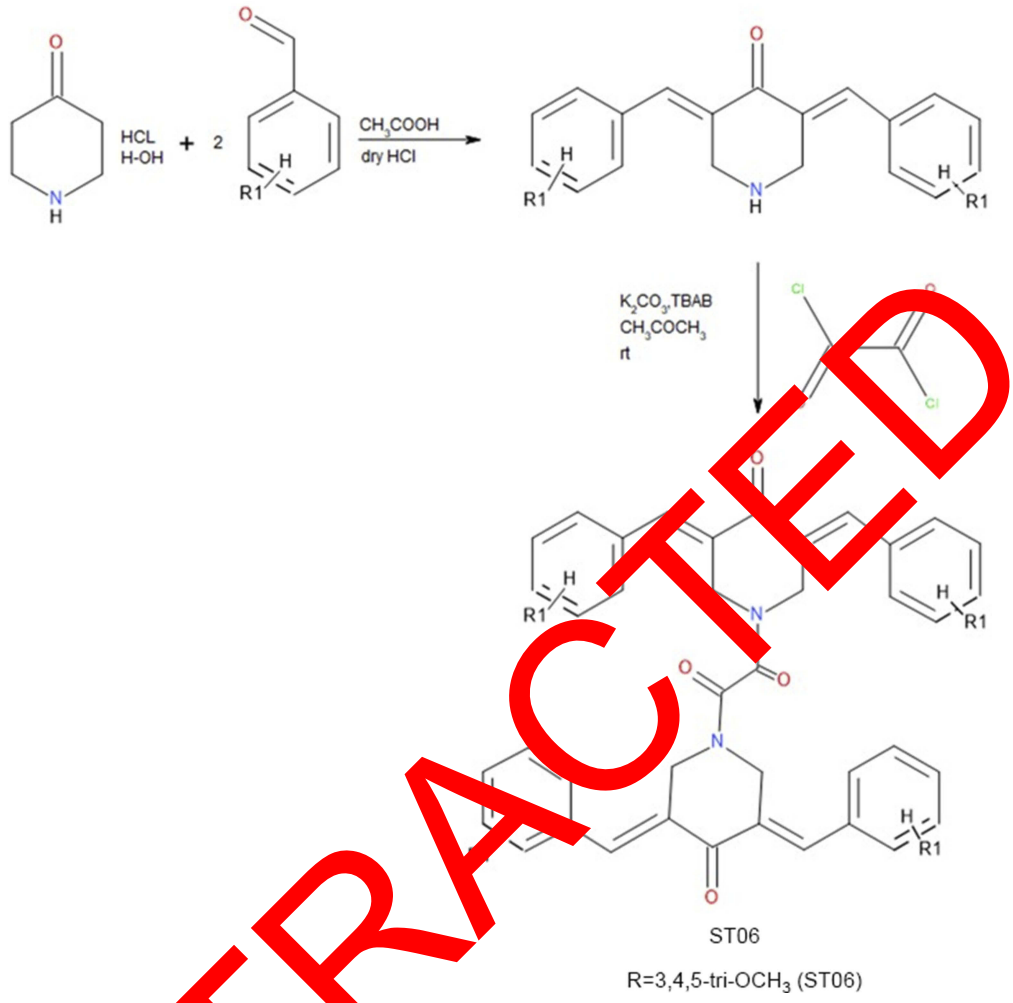

Figure S1 Schematic representation of the synthesis of ST06.
Notes: The reaction of 4-piperidone hydrochloride with 3,4,5, -trimethoxy benzaldehydes in the presence of dry hydrogen chloride yielded 3,4,5-bis(benzylidene)-4-piperidone. To the solution of 3,5- dibenzyledenepiperidin-4-one, potassium carbonate was added followed by addition of tetrabutyl ammonium bromide (TBAB) and oxalyl chloride to obtain 3,4,5-tri-OCH_3 (ST06). Das S, Das U, Varela-Ramirez A, et al. Bis[3,5-bis(benzylidene)-4-oxo-1-piperidinyl]amides: A novel class of potent cytotoxins. *ChemMedChem*. 2011.6.1892–1899. Copyright Wiley-VCH Verlag GmbH and Co. KGaA. Reproduced with permission.[1]

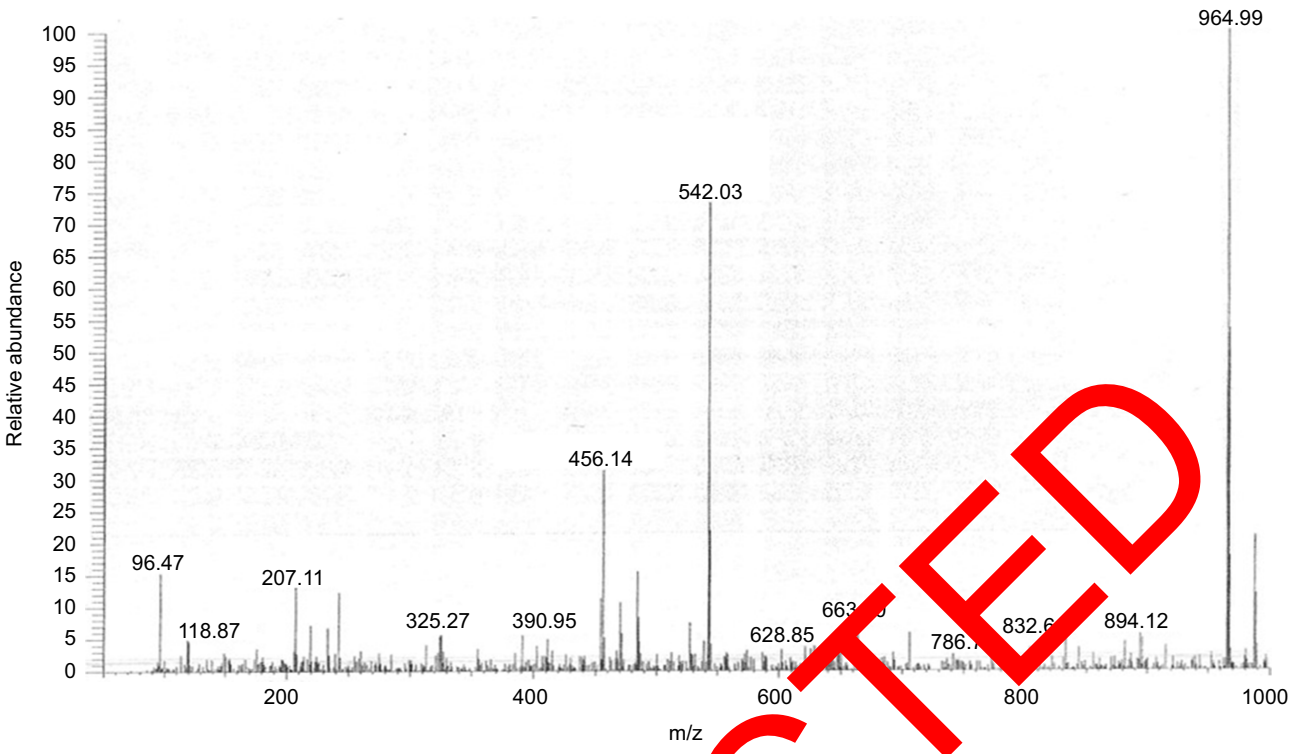

Figure S2 Mass Spectrometry data of ST06.
Notes: Representative chromatography of ST06 as obtained by Mass spectrometry (MS (ES… m/z: 964.99)

Reference

1. Das S, Das U, Varela-Ramirez A, et al. Bis[3,5-bis(be…ylidene)-4…xo-1-piperidinyl]amides: A novel class of potent cytotoxi… *Chem*… 2011;6(10):1892–1899. doi:10.1002/cmdc.201…0199